Analytica Chimica Acta 1402 (2026) 345392

Contents lists available at ScienceDirect

Analytica Chimica Acta

journal homepage: www.elsevier.com/locate/aca

Azetidination-based photocycloaddition enables regioisomer-resolved annotation of cholesteryl esters by negative-ion-mode LC-MS/MS

Andrea Cerrato [a,b], Enrico Taglioni [a,b], Chiara Cavaliere [a,b], Aldo Laganà [a,b], Elena Lucà [a], Carmela Maria Montone [a,b], Anna Laura Capriotti [a,b,*]

[a] Department of Chemistry, Sapienza University of Rome, Piazzale Aldo Moro 5, 00185, Rome, Italy
[b] Interuniversity Consortium INBB – Biostructures and Biosystems National Institute, Via dei Carpegna 19, 00165, Rome, Italy

HIGHLIGHTS

- Aza-Paternò-Büchi derivatization enables negative-ion-mode CE analysis.
- C═C regioisomers of cholesteryl esters resolved by aPB reaction and LC–MS/MS.
- Distinct fragmentation mechanisms identified for aPB-derivatized CE.
- Diagnostic product ions allow relative and absolute quantitation of CE regioisomers.
- CE regioisomer distributions determined in plasma and liver samples.

GRAPHICAL ABSTRACT

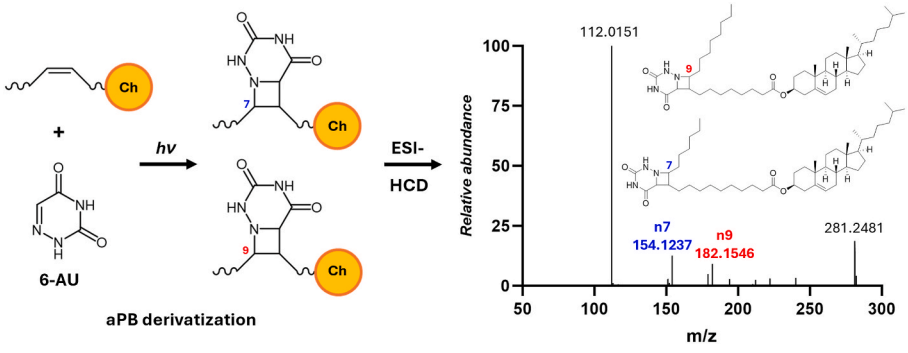

ARTICLE INFO

Handling Editor: Dr. L. Liang

Keywords:
Aza-Paternò-Büchi
Lipidomics
High-resolution mass spectrometry
Double bond location

ABSTRACT

Background: Cholesteryl esters (CE) play central roles in lipid transport and storage, yet their structural characterization remains challenging due to their extreme hydrophobicity and poor ionization efficiency. Conventional CE lipidomics workflows typically rely on positive-ion-mode analysis and report CE at the sum-composition level, without resolving double-bond (C]C) positional isomerism. Chemical derivatization strategies enabling isomer-resolved analysis of CE are therefore highly desirable but remain largely unexplored.
Results: In the present study, the use of the aza-Paternò-Büchi (aPB) reaction with 6-azauracil was extended to CE, enabling negative-ion-mode LC–HRMS/MS analysis with annotation of C]C bond regiochemistry. Optimization of the derivatization conditions allowed efficient reaction of highly hydrophobic CE while maintaining compatibility with electrospray ionization. Tandem mass spectrometry revealed a previously unreported set of diagnostic fragment ions that proved particularly suitable for quantitative applications. The workflow enabled both relative and absolute quantitation of CE regioisomers with good linearity, repeatability, and trueness over a wide dynamic range, using a single dominant diagnostic ion to simplify data processing. Application to complex biological matrices of clinical interest demonstrated the feasibility of the approach, providing direct access to CE regioisomer distributions in human plasma and bovine liver.

* Corresponding author. Department of Chemistry, Sapienza University of Rome, Piazzale Aldo Moro 5, 00185, Rome, Italy.
E-mail address: annalaura.capriotti@uniroma1.it (A.L. Capriotti).

https://doi.org/10.1016/j.aca.2026.345392
Received 29 January 2026; Received in revised form 10 March 2026; Accepted 11 March 2026
Available online 13 March 2026

Significance: This study establishes aPB-based derivatization as a viable and complementary strategy for structurally resolved CE analysis, expanding the analytical toolbox for lipidomics studies where detailed molecular structure is critical for biological interpretation.

1. Introduction

Cholesterol is a ubiquitous sterol lipid that fulfills multiple essential biological functions in mammalian systems. Besides representing a vital component of the cell membranes and being involved in cell signaling, it also functions as a precursor of several steroid hormones, bile acids, and vitamin D [1,2]. In mammalian cells, cholesterol exists either in its free, biologically active form or as cholesteryl esters (CEs), which represent an inert storage form. The balance between these two pools is tightly regulated by opposing metabolic processes. CEs are formed through esterification of the 3-hydroxyl group of cholesterol with fatty acids (FA), catalyzed by specialized enzymes. In mammalian tissues, CEs containing long-chain FA are widely distributed and constitute the primary form in which cholesterol is transported in the bloodstream [3]. Esterifying cholesterol makes it more suitable for storage and circulation, as the resulting CEs are more hydrophobic than free cholesterol. This property allows them to be efficiently enclosed within the hydrophobic core of lipoproteins, enabling their distribution throughout the body [4].

Because sterol homeostasis is fundamental for normal cellular function, CE metabolism plays a central role in maintaining intracellular free cholesterol levels. Dysregulation of CE synthesis or hydrolysis is associated with a variety of pathological conditions, including metabolic disorders [5], cardiovascular diseases [6], and various types of cancer [7–9]. Cancer cells, in particular, exhibit an increased demand for free cholesterol to support membrane biogenesis, proliferation, and tumor progression. This demand is satisfied through extracellular uptake, de novo biosynthesis, and, notably, hydrolysis of intracellular CE stores [10].

Within this context, high-resolution mass spectrometry (HRMS) has emerged as a powerful analytical tool for comprehensive lipidome characterization. The development of novel tandem mass spectrometry (MS/MS) methods, particularly in configurations such as shotgun analysis [11] or LC-HRMS [12], has become a valuable resource for characterizing biomolecules at high sensitivity. HRMS-based untargeted lipidomics represents the most appropriate route for maximizing the number of identified lipid structures and uncovering potential disease-associated markers. Accordingly, detailed molecular profiling of CEs can provide valuable insight into changes in CE composition across different biological conditions, supporting the discovery of lipid-based markers.

Although CEs are composed of only two structural components, they display substantial molecular diversity, arising from variations in fatty acyl chain length (C0–C40) and degree of unsaturation (0–8 carbon–carbon double bonds) [13]. CEs are commonly analyzed using electrospray ionization mass spectrometry (ESI-MS) in positive ion mode, where abundant adduct ions such as $[M + NH_4]^+$, $[M+Na]^+$, or $[M+Li]^+$ are formed and subjected to low-energy collision-induced dissociation (CID) [14–16]. In this regard, MS/MS of CE adduct ions via CID provides a characteristic and abundant cholesteryl core cation ($[Chol + H - H_2O]^+$, *m/z* 369.3516), which is generally employed for the identification and quantification of CEs.

Growing evidence suggests that lipid regioisomerism plays a crucial role in distinguishing pathological states from controls [17,18]. However, conventional CID-based approaches are unable to localize carbon–carbon double bonds within unsaturated fatty acyl chains, as gas-phase cleavage of nonpolar C–C or C═C bonds in even-electron lipid ions is energetically unfavorable. Consequently, the structural resolution of most MS-based lipidomics platforms rarely exceeds the fatty acyl composition level, leaving ambiguities among lipid isomers that differ only in double-bond position, geometry, or regiochemistry [19].

To address these limitations, several innovative approaches for pinpointing carbon–carbon double bonds have been proposed, including fragmentation techniques alternative to CID [20,21], gas phase molecule/ion reactions [22,23], and chemical derivatization [18,24–27]. Chemical derivatization approaches gained popularity among researchers because they do not require any hardware modification, which enhances compatibility with routine LC-HRMS lipidomics. The group of Xia first reported the applications of the Paternò-Büchi (PB) photocycloaddition reactions for assigning the regiochemistry of C═C bonds in CEs. In their first study [28], employing acetone as both PB reagent and cosolvent, CID MS/MS of the PB products of CEs as $[M+ Li]^+$ adduct ions provided information of the fatty acyl composition, while subsequent MS^3 CID of the acetone-modified fatty acyl moieties generated diagnostic ions for locating carbon-carbon double bonds. In their following study, they used 2-acetylpyridine as charge-tagging PB reagents to overcome the limited sensitivity encountered with lithium ion adducts [29]. Recently, unsaturated CE were structurally characterized through chemical derivatization using an N-methyl aziridination reagent, which resulted in an increased sensitivity in positive ion mode, as well as allowing confident structural resolution of positional regioisomers [30].

Despite the large body of literature concerning chemical derivatization by the PB reaction and its variants, most studies were based on CID fragmentation rather than higher-collisional dissociation (HCD). Recently, our group has demonstrated that the aza-Paterno-Büchi (aPB) reaction with 6-azauracil (6-AU) and HCD under negative ion mode ESI (−) is suitable to effectively pinpoint carbon-carbon double bond location in fatty acyl chains of free FA and GP in complex, lipid-rich matrices [31–33]. In the present work, we aimed to expand the applicability of aPB derivatization to neutral and apolar lipids by introducing a novel LC-MS/MS platform dedicated to CE structural characterization in negative ion mode under HCD conditions. To the best of our knowledge, this is the first report of the use of negative ionization HRMS for the annotation and quantitation of CE.

2. Materials and methods

2.1. Chemicals and reagents

Optima mass spectrometry (MS) grade water, methanol (MeOH), and isopropanol (iPrOH) were purchased from Thermo Fisher Scientific (Waltham, MA, United States). Glacial acetic acid, ammonium acetate, 6-AU, chloroform, and ethanol (EtOH) were purchased from Merck (Darmstadt, Germany). Cholesteryl oleate (CE 18:1 n9), cholesteryl vaccenate (CE 18:1 n7), cholesteryl petroselinate (CE 18:1 n12), cholesteryl linoleate (CE 18:2 n6), cholesteryl palmitoleate (CE 16:1 n7), and cholesteryl arachidonate (CE 20:4 n6) were purchased from Larodan AB (Solna, Sweden). Phree cartridges were provided by Phenomenex (Torrance, CA, USA). Human plasma reference material was purchased from Merck (Darmstadt, Germany). Human pancreatic cancer cell lines (Aspc-1) were purchased from American Type Culture Collection (ATCC, Rockville, MD, USA). Bovine liver was purchased from a local market in Rome, Italy.

2.2. Lipid extraction

CE extraction was carried out following a modified version of the extraction method performed by Bligh and Dyer (B&D) in a 1:10 sample-

to-solvent ratio [34]. Briefly, human plasma (100 μL) was added to 305 μL of MeOH and vortexed for 2 min at room temperature. Then, 305 μL of $CHCl_3$ was added, and the mixture was vortexed for 2 min at room temperature. Finally, 290 μL of H_2O was added to the tubes. The final mixture was kept vortexing for 20 min. Samples were centrifuged at 3000×*g* at 4 °C for 15 min, allowing for phase separation. The lower layer was carefully removed using a Pasteur pipette and subsequently split into two (200 μL equivalent) for underivatized lipidomics and further derivatization before evaporation with a Speed-Vac SC 250 Express (Thermo 164 Avant, Holbrook, NY, USA). As regards bovine liver extraction, 100 mg of liver tissue was homogenized and extracted using a modified B&D extraction as described for human plasma. Aspc-1 cells were maintained in Dulbecco Modified Eagle Medium (DMEM) (Gibco Life Technologies) supplemented with 2 mM L-glutamine, 100 IU/mL penicillin/Streptomycin and Fetal Bovine Serum (FBS) (Gibco Life Technologies) 10% and under a humidified atmosphere at 37 °C and 5% CO_2. Briefly, cells were detached and dispensed at a density of 3×10^6 cells per Falcon 5 mL round-bottom polystyrene test tube. After a 3 min centrifugation at 1000 rpm at 4 °C, the obtained cell pellet was resuspended in 100 μL of PBS. Resuspended cell pellets were extracted following the B&D protocol as well.

Samples intended for underivatized lipidomics were reconstituted in 250 μL of MeOH/iPrOH/$CHCl_3$ (47.5:47.5:5, *v/v/v*) and filtered prior to injection. Aliquots designated for aPB derivatization were subjected to phospholipid removal using Phree™ cartridges (Phenomenex, Torrance, CA, USA), centrifuged at 3000×*g* for 10 min at room temperature, and the filtrate was collected for derivatization.

2.3. Offline aPB reaction

CE stock solutions were prepared in pure EtOH/$CHCl_3$ (90/10, *v/v*) at 1.5 mmol L^{-1} 6-AU was dissolved in EtOH (24 mmol L^{-1}). CE standards and 6-AU were dissolved in 1 mL of EtOH/H_2O/$CHCl_3$ (94:5:1, *v/v/v*) for the aPB reaction with final concentrations of 0.1 mmol L^{-1} and 10 mmol L^{-1}, respectively. Then, they were placed in a quartz cuvette and purged with nitrogen gas to remove residual oxygen. The cuvette was irradiated at 254 nm using a Spectroline E-series UV lamp with shortwave emission (Thermo Fisher Scientific) for 30 min at room temperature. Next, a 200 μL aliquot of the resulting reaction mixture was subjected to further UHPLC-HRMS analysis. Aliquots of 200 μL of each phospholipid-free lipid extract from human plasma, cell lines, and bovine liver were dissolved in 2 mL of EtOH/H_2O/$CHCl_3$ (90:5:5, *v/v/v*) for the aPB reaction. Moreover, 50 μmol L^{-1} CE 18:1 n-12 was added as an internal standard for absolute quantitation. The quartz cuvette was purged with nitrogen gas to remove residual oxygen and exposed to 254 nm radiation for 30 min at room temperature. Reaction mixtures were dried with a Speed-Vac SC 250 Express and finally reconstituted with 250 μL of MeOH/iPrOH/$CHCl_3$ (47.5:47.5:5, *v/v/v*) into a glass vial before UHPLC-HRMS analysis. All experiments were performed in triplicate.

2.4. UHPLC-HRMS analysis and CE annotation

CE separation was carried out by a Vanquish binary pump H (Thermo Fisher Scientific, Bremen, Germany), equipped with a thermostated autosampler and column compartment, on a C18 Hypersyl GOLD (50 × 2.1 mm, 5 μm particle size; Thermo Fisher Scientific) at 50 °C with a flow rate of 300 μL min^{-1}. The mobile phases consisted of H_2O/MeOH/CH_3COOH (49.8:49.9:0.15, *v/v/v*) with 5 mmol L^{-1} CH_3COONH_4 (phase A) and MeOH/iPrOH/CH_3COOH (49.9:49.9:0.15, *v/v/v*) with 5 mmol L^{-1} CH_3COONH_4 (phase B). The chromatographic gradient was as follows: 4 min at 40% phase B, from 40 to 60% phase B in 2 min, from 60 to 99% phase B in 10 min, 99% phase B for 6 min (washing step), 99 to 40% phase B in 2 min, and 40% phase B for 6 min (equilibration step). The injection volume was 10 μL. The UHPLC system was coupled to the Q Exactive hybrid quadrupole-Orbitrap mass spectrometer (Thermo Fisher Scientific) with the following source settings in negative ion mode ESI (−): spray voltage 2.5 kV; capillary temperature 320 °C; sheath gas flow rate 35 arbitrary units (a.u.); auxiliary gas flow rate 25 a.u.; auxiliary gas heater temperature 400 °C. The same parameters were set for positive ion mode. Full-scan MS data were acquired in the range of 200−1200 *m/z* with a resolution (full width at half maximum, FWHM) of 35,000. The automatic gain control (AGC) target value was 500,000, and the maximum ion injection time was 200 ms. The isolation window width was 2 *m/z*. TOP 5 data-dependent acquisition (DDA) MS/MS fragmentation was performed with a resolution (FWHM) of 17,500. AGC target value was set at 100,000, and dynamic exclusion was set to 2 s. Collision energy fragmentation was achieved in the HCD cell at 30 NCE. Raw data files were acquired by Xcalibur software (version 3.1, Thermo Fisher Scientific). Raw data from three consecutive injections were obtained for each sample. Underivatized CE precursors were manually searched in the underivatized sample MS data based on the LIPID MAPS database. CEs were putatively identified and annotated by careful inspection of the MS/MS spectra based on known CE fragmentation patterns. Subsequently, aPB reaction products (corresponding to a relative mass shift of +113.0225) were manually searched in the derivatized sample MS data. Diagnostic product ions and relative abundances of annotated lipid isomers were evaluated.

2.5. Statistical analysis

Statistical analysis was performed with GraphPad Prism 10.2 (GraphPad Software, La Jolla, CA, USA). *t*-Test analyses were performed, and data were reported as bar charts with error bars and statistical significance: ns (nonsignificant), * ($p < 0.1$), ** ($p < 0.01$), *** ($p < 0.001$), or **** ($p < 0.0001$).

3. Results and discussion

3.1. Setup of the aPB derivatization

The aPB photocycloaddition of 6-AU and polar lipid classes has previously been demonstrated as an effective strategy in generating lipid derivatives that yield diagnostic product ions for C=C regiochemistry assignment upon HCD fragmentation in negative ion mode [31–33]. In addition to the reactive imine functionality required for photocycloaddition, the 6-AU moiety introduces an ionizable imide group with acidity comparable to that of phenolic compounds, which are routinely analyzed in negative ion mode [35], thereby substantially enhancing ionization efficiency under negative electrospray conditions. This behavior was clearly exemplified by the ionization properties of aPB-derivatized glycerophosphatidylcholines (PC). Whereas non-derivatized PC undergo in-source fragmentation of the quaternary ammonium when subject to ESI ionization in negative ion mode, their derivatized counterparts were efficiently ionized as deprotonated adducts [31].

Thus, the aPB derivatization with 6-AU appeared to be a promising candidate for extending negative-ion-mode isomer-resolved lipidomics for CE, a class of lipids that is even less prone to ionization in negative ion mode due to the absence of functional groups that can be deprotonated. However, the application of this chemistry to extremely hydrophobic analytes introduces significant practical challenges arising from the markedly different physicochemical properties of the reactants. Whereas 6-AU is a highly polar compound ($XlogP_3 = -0.6$) and readily soluble in aqueous and alcoholic solvents, cholesteryl esters exhibit extreme hydrophobicity ($XlogP_3 = 16.6$ for CE 18:1) and require nonpolar solvents, such as chloroform or aromatic hydrocarbons, for efficient solubilization, and stock solutions had to be prepared in EtOH/$CHCl_3$ (90:10, *v/v*). Consequently, careful optimization of the reaction solvent system was necessary to ensure sufficient solubility of both reaction partners while maintaining compatibility with the aPB photocycloaddition.

A first set of experiments was performed to define the reaction solvent (Fig. 1A). The previously optimized aPB conditions for polar lipids (MeOH/H_2O, 70:30, *v/v*) were initially tested; however, the reaction mixture became turbid, and no signal corresponding to the derivatized CE was detected. This behavior was attributed to the poor solubility of CE in highly polar solvent systems. To improve CE solubilization while maintaining compatibility with 6-AU, the derivatization protocol was modified by dissolving 6-AU in ethanol and comparing acetone, ethanol, and isopropanol as reaction solvents. Solvents more hydrophobic than iPrOH (e.g., dimethyl ether) were not suitable due to the immediate precipitation of 6-AU. Among the tested solvents, ethanol provided the highest peak areas for the aPB-derivatized CE 18:1 species and was therefore selected as the reaction solvent.

Subsequently, the effect of $CHCl_3$ and H_2O content in the reaction mixture was evaluated. Chloroform was required to ensure adequate solubilization of CE standards and efficient extraction from complex biological matrices, whereas the presence of water has been previously reported to influence 6-AU reactivity [36]. As shown in Fig. 1B, the $CHCl_3$ content (0.5-5 % in EtOH) did not have a significant effect on the peak area of the aPB derivatized CE 18:1. However, a small increasing trend could be noticed (in particular if 0.5 and 5% were compared), possibly due to an improvement in the CE solubilization. These results were critical, as a $CHCl_3$ content of 5% in the solvent mixture was required to enable straightforward coupling of CE extraction from complex matrices with the subsequent derivatization step. Conversely, the addition of water (from 99:1 EtOH/$CHCl_3$ to 89:10:1 EtOH/-H_2O/$CHCl_3$) significantly enhanced the peak area of the derivatized CE once the water content exceeded 2% (Fig. 1C). Based on these results, a solvent composition of 90:5:5 EtOH/$CHCl_3$/H_2O (*v/v/v*) was selected for subsequent experiments. This mixture represents a compromise between maximizing derivatization efficiency and ensuring adequate solubilization of CE. By comparing the peak areas of underivatized CE after aPB derivatization with those from a control reaction (CE exposed to UV light without 6-AU), the reaction conversion was estimated to be approximately 20–25%, regardless of the CE analyzed. This value may represent a slight overestimation, as the calculation does not account for the formation of minor reaction byproducts. The observed conversion is consistent with previous reports for free FA and glycerophospholipids [31].

3.2. Fragmentation mechanisms of aPB-derivatized CE

Once the reaction conditions were adjusted, individual CE were derivatized and analyzed by LC-HRMS to confirm the applicability of aPB for the regiochemical assignment of C=C bonds in CE. Owing to the intrinsic asymmetry of both 6-AU and C=C bonds on fatty acyl chains, aPB derivatization yields two distinct derivatives for each double bond (P1 and P2). In the case of free FA, each aPB product undergoes characteristic cleavage of the azetidine ring upon HCD fragmentation in negative ion mode, generating a pair of complementary diagnostic ions (F1 and F2) that enable unambiguous localization of the C=C position (Fig. S1A) [31]. This behavior is analogous to that observed for classical PB derivatives formed with ketone reagents [24]. For example, the aPB derivatives of FA 18:1 n9 generate two diagnostic product ions at *m/z* 223.1449 (F1) and 182.1189 (F2), whereas FA 18:1 n7 yields ions at *m/z* 195.1138 (F1) and *m/z* 210.1498 (F2) (Fig. S1B–C), in addition to the very intense ion of 6-AU at 112.0151. When fatty acids are esterified to glycerophospholipids, diagnostic ion formation proceeds through initial cleavage of the ester bond, releasing aPB-derivatized FA that subsequently fragment to yield F1 and F2 ions. By contrast, PB-derivatized GP analyzed in positive ion mode generate diagnostic information through characteristic neutral losses of the modified acyl chains [24,37].

Fig. 2A shows the MS/MS spectrum of the aPB derivatives of CE 18:1 n9 in the *m/z* range 50-300. The spectrum shows the canonical diagnostic ions F1 and F2 observed in the spectra of free FA and GP, and the complete MS/MS spectrum also displays ions corresponding to aPB-derivatized free FA 18:1 (*m/z* 394.2716, 376.2598, and 351.2646, Fig. S2). Notably, two additional fragment ions at *m/z* 182.1546 and 212.1291 were observed at significantly higher abundance than the expected F1 and F2 ions. At 30 NCE, no other intermediate ions were detected that could readily suggest a plausible fragmentation pathway leading to these species.

To further investigate this alternative fragmentation pathway, aPB-derivatized CE 18:1 n-9 was therefore analyzed across a range of collision energies (10–40 NCE). The intensities of *m/z* 394.2716, 223.1449 (F1), and 182.1546 were then evaluated across the range of collision energies (Fig. S3). The precursor-related ion at *m/z* 394.2716 rapidly increased in intensity, reaching a maximum at NCE 20–25, and subsequently decreased at higher energies. In contrast, the F1 ion (*m/z* 223.1449) began to increase at NCE ≥25 and reached its maximum intensity at NCE 35, confirming that its formation occurs downstream of the *m/z* 394.2716 species. The comparable intensity profiles of these two ions further support their involvement in a common fragmentation pathway that was schematized in Fig. S4. Conversely, the ion at *m/z* 182.1546 was approximately an order of magnitude more intense and exhibited a markedly different energy-dependent trend, suggesting that it originates from an alternative and independent fragmentation mechanism. Despite the broad range of NCE values investigated, no additional intermediate ions were detected. In particular, for both F3 and F4 generation, no evidence of prior urea loss (at *m/z* 702.5818 for CE 18:1) was observed, nor loss of the terminal side of the fatty acyl chain for F4 (*m/z* 574.4253). Unlike F1 and F2, which originate from ester bond cleavage followed by FA-like dissociation, F3 and F4 appear to arise directly from both P1 and P2 through a fragmentation pathway consistent with a

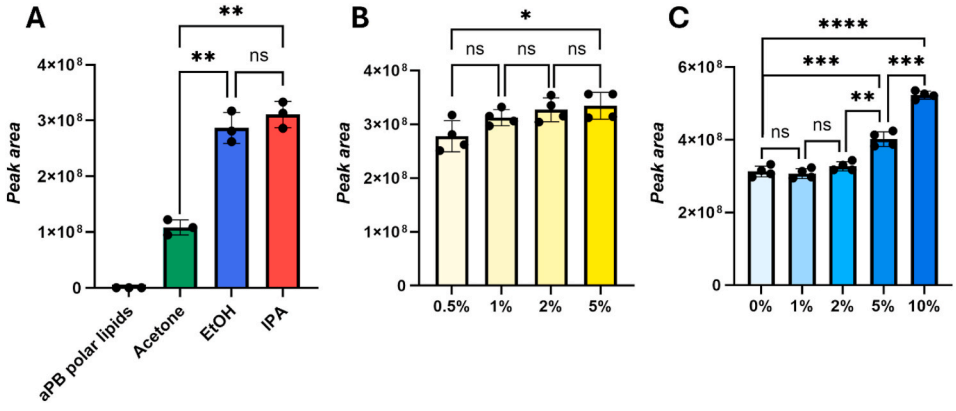

Fig. 1. Bar charts comparing the peak areas of aPB derivatized CE 18:1 n9 based on reaction solvent (A), $CHCl_3$ content (B), and water content (C). *t*-test analysis was performed: ns, $p > 0.1$; *, $p < 0.1$; **, $p < 0.01$; ***, $p < 0.001$; ****, $p < 0.0001$.

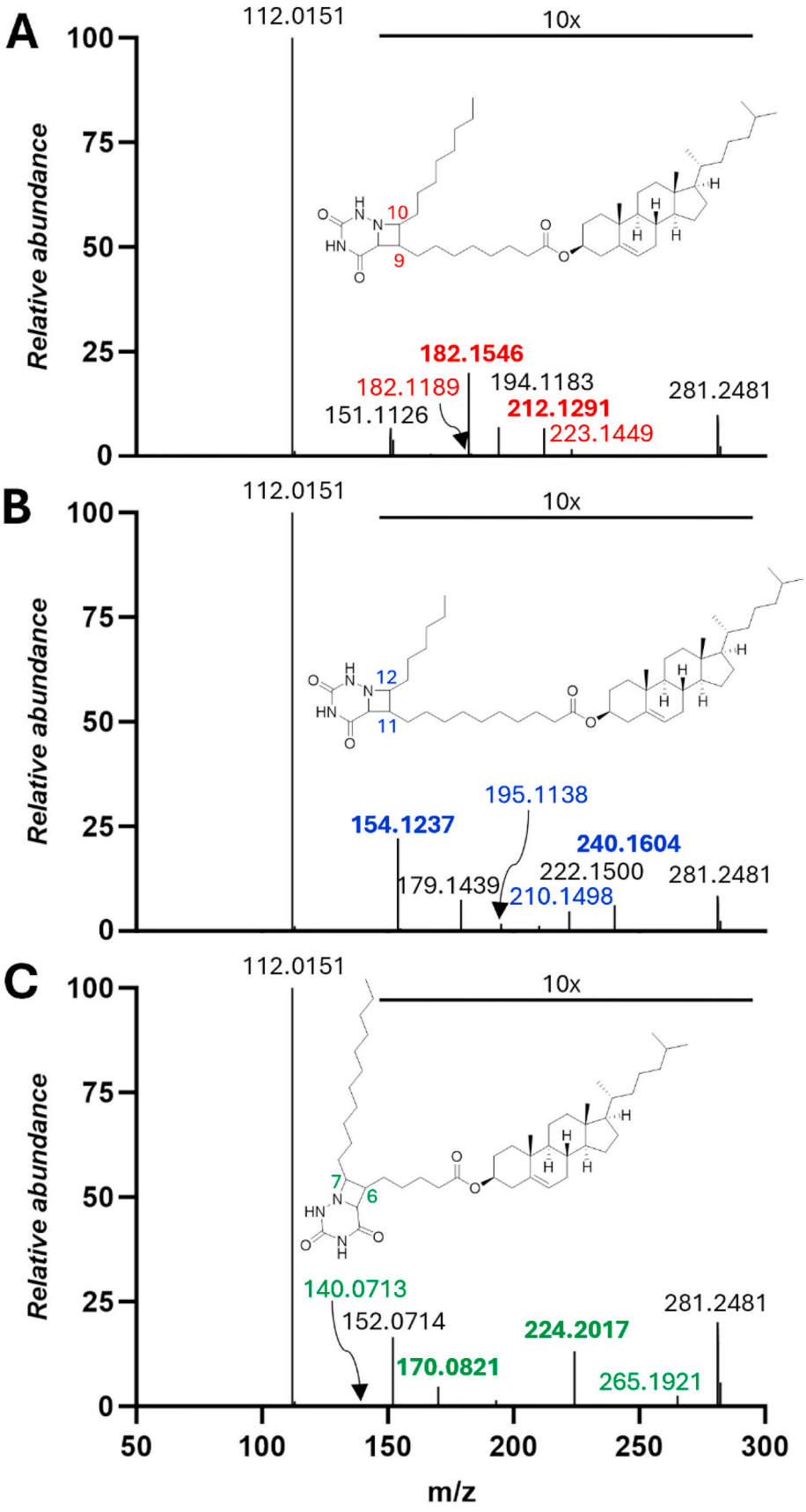

Fig. 2. ESI- MS/MS spectra in the range 50-300 *m/z* of the aPB derivatives of CE 18:1 n9 (A), CE 18:1 n7 (B), and CE 18:1 n12 (C).

concerted mechanism that was hypothesized and schematized in Fig. S5, which can rationalize the formation of F3 (*m/z* 182.1546) and F4 (*m/z* 212.1291), respectively. Both fragments arise from analogous cleavages along the N–CH–CO bonds linking the azetidine and uracil rings, with F3 retaining the terminal portion of the fatty acyl chain and F4 bearing the carboxyl group. This assignment is further supported by the prominent water loss observed for F4, yielding the fragment ion at *m/z* 194.1183. Although this interpretation is strongly supported by the observed fragmentation behavior and energy-resolved experiments, definitive confirmation of the exact bond cleavages and charge retention sites would require additional experiments such as MS^3 or isotopic labeling, which were beyond the scope of the present study.

Finally, a peak at *m/z* 480.3573 can be noticed in Fig. S2 arising from a neutral loss of 282.2570 (oleic acid). This peak demonstrates the formation of a third minor aPB derivatization product (P3), deriving from the derivatization of the much more sterically hindered unsaturation on the cholesterol moiety. The presence of a third minor derivatization product did not interfere with the interpretation of CE fatty acyl C═C regiochemistry.

The MS/MS spectra of CE 18:1 n7 and n12 (Fig. 2B–C) confirmed the hypothesized fragmentation pathways with four diagnostic product ions, two of which (F3 and F4) were significantly more intense. In addition to the expected F1 and F2 ions, which are common to free FA 18:1 n7 (Fig. S1C), aPB-derivatized CE 18:1 n7 displayed intense F3 and F4 ions (*m/z* 154.1237 and 240.1604), which were approximately 28 Da lower and higher (two CH_2 units), respectively, than those observed for the n9 isomer. Similarly, the F3 and F4 ions of CE 18:1 n12 were approximately 42 Da higher and lower (three CH_2 units), respectively, than those of the n9 isomers. These mass shifts provide further proof that F3 bears the terminal side of the fatty acyl chain whereas F4 retains the carboxyl side. Accordingly, CE 16:1 n7, which shares the carboxyl side with CE 18:1 n9 and the terminal side with CE 18:1 n7, exhibited F1 and F3 ions in common with the latter and F2 and F4 ions in common with the former (Fig. S6A).

Later, polyunsaturated CE were analyzed, i.e., CE 18:2 n6, CE 18:3 n6, and CE 20:4 n6 (Fig. S6B–D). As expected, the number of diagnostic peaks increased with the number of unsaturations, e.g., in the case of CE 18:2 n6, two F1 ions (*m/z* 181.0982 and 221.1232) and two F3 ions (*m/z* 140.1079 and 180.1391) were present, with a mass difference of around 40 Da (CH_2–CH═CH). Despite the increased number of ions and the subsequent decrease of the ion intensities, the interpretation of CE fatty acyl C═C regiochemistry is independent of the number of unsaturations. The only difference between mono- and polyunsaturated CE is represented by a less pronounced preference of the latter for the concerted mechanism over the one mediated by the cholesteryl ester bond cleavage, possibly due to the enhanced stabilization of the double bonds on aPB derivatized free FA. In a further experiment, equimolar CE 18:1 n9, CE 18:1 n7, CE 18:2 n6, and CE 18:3 n6 were simultaneously derivatized and analyzed to evaluate the applicability of the reaction on complex mixtures comprising mono- and polyunsaturated CE. The results showed no apparent selectivity of the reaction with respect to the number of double bonds, as comparable conversions (measured in terms of peak areas) were observed.

3.3. Relative and absolute quantitation of CE regioisomers

Relative quantitation was evaluated by derivatizing mixtures of CE regioisomers while maintaining a constant total concentration (0.1 mmol L^{-1}). CE 18:1 n9 and n7 were analyzed at 6 M ratios (n9/n7 = 49, 19, 9, 3, 1, and 0.5). Thus, the intensities of the diagnostic ions (F1–F4) were annotated, and the ratios of their summed intensities (I_{n9}/I_{n7}) were plotted against the corresponding molar ratios (C_{n9}/C_{n7}) on the logarithmic scale to build a linear regression. Excellent linearity (R^2 = 0.9988) was obtained over a dynamic range spanning two orders of magnitude (Fig. S7). Given the prevalence of the F3 ion over the three other fragments, a second regression model was constructed using only the F3 intensity ratio between the two isomers (Fig. 3A), which resulted in improved linearity (R^2 = 0.9991). This simplified approach was therefore preferred, as it substantially reduces data annotation complexity. The slope of the regression was close to unity (1.036), indicating similar reactivity and gas-phase fragmentation behavior for the two isomers, and suggesting that their molar ratio can be reasonably estimated directly from the diagnostic peak ratio. Analogous experiments were repeated for isomeric CE 18:1 n9 and the non-naturally present isomer n12 using the same molar ratio. The logarithmic plot of intensity ratios versus concentration ratios again showed excellent linearity (R^2 = 0.9982, Fig. S8).

To assess the applicability of the aPB reaction for absolute CE

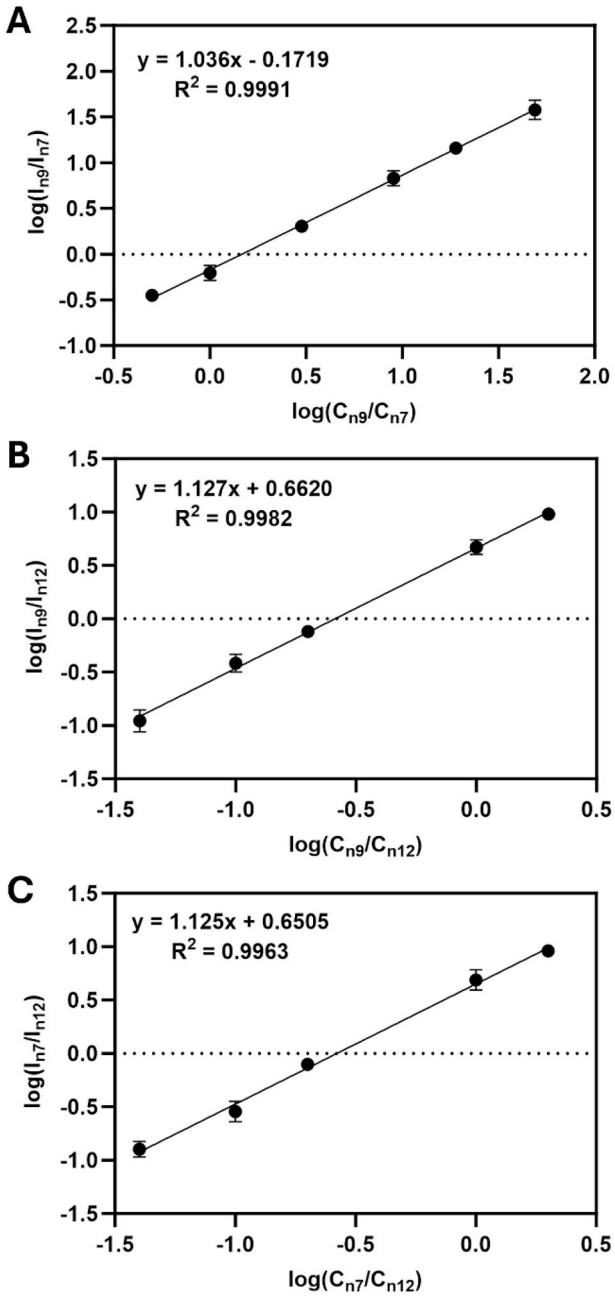

Fig. 3. Relative and absolute quantitation of CE 18:1 n9 and n7. (A) plot of the intensity ratios (I_{n9}/I_{n7}) of the F3 ions (*m/z* 182.1546 and 154.1237) against their molar ratios (C_{n9}/C_{n7}), (B) plot of the intensity ratios (I_{n9}/I_{n12}) of the F3 ions (*m/z* 182.1546 and 224.2017) against their molar ratios (C_{n9}/C_{n12}), (C) plot of the intensity ratios (I_{n7}/I_{n12}) of the F3 ions (*m/z* 154.1237 and 224.2017) against their molar ratios (C_{n7}/C_{n12}).

quantitation, a series of experiments were conducted using CE 18:1 n9 or n7 at five different concentrations (2, 5, 10, 50, and 100 μmol L^{-1}) and CE n12 at a fixed concentration (50 μmol L^{-1}) as an internal standard. Similar to the relative quantitation models, the ratios of the intensities of the F3 ions were plotted against the molar ratios to build regression models. Both analytes exhibited strong linearity ($R^2 = 0.9982$ for n9 and 0.9963 for n7) across a wide dynamic range (Fig. 3B and C).

Analytical performance was further evaluated in terms of precision and trueness. Precision was evaluated from four independent derivatization and analysis replicates. The relative standard deviation (RSD) of the F3 diagnostic ion response ranged from 3.9 to 8.5% across the three CE 18:1 regioisomers. At 50 μmol L^{-1}, RSD values of 3.9%, 8.5%, and 8.0% were obtained for CE 18:1 n9, n7, and n12, respectively, indicating good repeatability of the aPB-based workflow. Trueness was evaluated by back-calculation of concentrations from the calibration curves and comparison with nominal values. For CE 18:1 n9, relative errors ranged from −8.3% to +10.2% across the 2–100 μmol L^{-1} range. For CE 18:1 n7, relative errors ranged from −11.6% to +10.7%. These results indicate acceptable trueness across the full working range, with no evidence of systematic bias. Finally, the limits of detection (LOD) and quantitation (LOQ) were evaluated. Since absolute quantitation was based on ion intensities rather than peak areas, conventional S/N-based approaches for estimating LOD/LOQ are not directly applicable. Instead, the analytical sensitivity of the method was evaluated from the calibration models using the regression-based approach (LOD = 3.3σ/S; LOQ = 10σ/S), where σ represents the standard deviation of the regression and S the slope of the calibration curve. The calculated values indicate that the aPB-based workflow enables reliable detection and quantitation of CE regioisomers in the low micromolar concentration range, i.e., for CE 18:1 n9 LOD was 1.9 μmol L^{-1} and LOQ was 5.7 μmol L^{-1}, whereas for CE 18:1 n7 LOD was 1.7 μmol L^{-1} and LOQ was 5.1 μmol L^{-1}.

3.4. Profiling of CE regioisomers in complex samples

Having established the analytical performance of the aPB-based workflow for CE, its applicability to complex biological matrices was evaluated using human blood, bovine liver, and human pancreatic cells. Bovine liver was chosen as a model for human tissue. Following B&D extraction, the organic layer was subjected to phospholipid removal using Phree™ cartridges. Despite the standard procedure of these cartridges being based on simultaneous protein precipitation and phospholipid removal (before B&D extractions), preliminary experiments on human plasma demonstrated that the B&D/Phree protocol yielded significantly higher CE peak areas than the Phree/B&D (Fig. S9). Based on the content of $CHCl_3$ in the organic phase, the reaction mixture in 2 mL had a final concentration of 5% $CHCl_3$ as discussed in paragraph 3.1, thereby enabling straightforward coupling between extraction and derivatization.

Fig. 4 displays the MS/MS spectrum of aPB-derivatized CE 18:1 from human plasma. In addition to the F3 ion of the internal standard n12 isomer (*m/z* 224.2017), three diagnostic F3 ions corresponding to endogenous CE 18:1 regioisomers were observed at *m/z* 182.1546 (n9), 154.1242 (n7), and 140.1079 (n6). Quantitation based on the regression model in Fig. 3A yielded an n9/n7 ratio of 18 ± 2 across three independent replicates. Absolute concentrations of the n9 and n7 isomers were determined to be 351 ± 23 and 27 ± 4 μmol L^{-1}, respectively, in excellent agreement with previously reported plasma values (325 ± 21 and 23 ± 2 μmol L^{-1}) [29]. Owing to the structural similarity and comparable fragmentation behavior, the regression curve established for the n7 isomer was also used to estimate the concentration of the minor n6 isomer, which was determined to be 7 ± 2 μmol L^{-1}.

In bovine liver, the MS/MS spectrum of aPB-derivatized CE 18:1 displayed the F3 ions of n9 and n7 isomers, in addition to the internal standard. Compared to human plasma, the n9/n7 ratio was markedly lower (4 ± 1). This observation is consistent with previous reports showing elevated levels of FA 18:1 n7 in animal liver compared to other

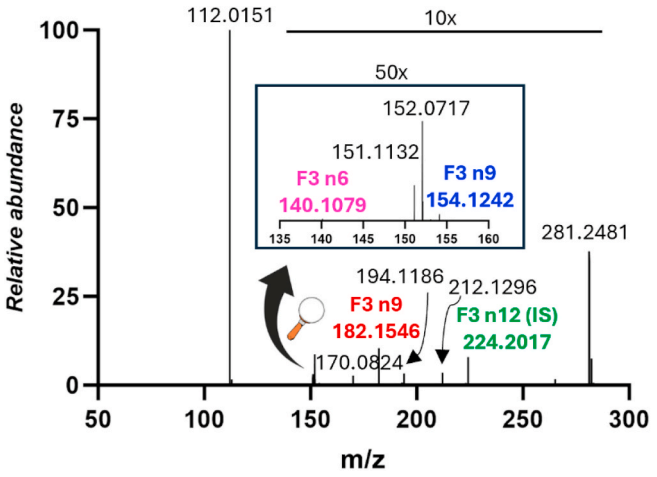

Fig. 4. ESI- MS/MS spectra in the range 50-300 *m/z* of the aPB derivatives of CE 18:1 from human plasma. Diagnostic F3 ions are marked in bold, i.e., *m/z* 140.1079 (n6), 154.1242 (n7), 182.1546 (n9), and 224.2017 (n12, internal standard).

tissues [38]. Absolute concentrations were determined to be 34.5 ± 2.6 and 10.4 ± 2.0 μg g^{-1}, for the n9 and n7 isomers, respectively. In contrast, analysis of CE 18:1 from Aspc-1 cells did not did not reveal detectable endogenous diagnostic ions beyond those of the internal standard, suggesting that CE 18:1 levels in this cell line are below the detection limits of the workflow, in agreement with previous studies that indicated a limited neutral lipid storage capacity of pancreatic cancer cell models.

In contrast, analysis of CE 18:1 from Aspc-1 cells did not did not reveal detectable endogenous diagnostic ions beyond those of the internal standard, suggesting that CE 18:1 levels in this cell line are below the detection limits of the workflow, in agreement with previous studies that indicated a limited neutral lipid storage capacity of pancreatic cancer cell models [39].

As expected, CE 18:2 constituted predominantly of the regioisomer n6, even though traces of the n3 isomer (roughly 1%) were detected in both human plasma and bovine liver (but not in the Aspc-1 cells), as evidenced by the diagnostic F3 ion at *m/z* 98.0611. Conversely, the isomers of CE 18:3 were only annotated in human plasma, resulting in a n6/n3 ratio around 3 (roughly estimated by the F3 intensity ratios), as previously found by Xie [29]. In both human plasma and bovine liver, CE 20:4, CE 20:5, and CE 22:6 were constituted by a single regioisomer, n6, n3, and n3, respectively. Moreover, plasma CE 16:1 was mainly constituted by the n7 isomer with traces of the n9 regioisomer.

Interestingly, three saturated CE were also annotated as minor aPB derivatives. Fig. S10 displays the MS/MS spectrum of aPB derivatized CE 16:0. In addition to the ions corresponding to 6-AU (*m/z* 112.0151) and free FA 16:0 (*m/z* 255.2329), there was an intense ion at *m/z* 480.3572, corresponding to aPB-derivatized cholesterol. This confirms the hypothesis of the derivatization of the C=C bond on the cholesterol structure that was also described in paragraph 3.2 for unsaturated CE.

In terms of CE coverage, our numbers are comparable to most lipidomics studies that report CE at the sum-composition level, without resolving the underlying double-bond regioisomer distributions. For example, Gowda et al. reported 8 CE species in plasma (7 unsaturated) [40], Gerl et al. reported 17 CE (12 unsaturated) [41], and Vaňková et al. reported 14 CE species [42]. Similarly, Sun et al. annotated 9 CE sum compositions in rat liver [30]. However, it should be noted that there have been studies in which charge-tagging reagents or advanced MS approaches resulted in an enhanced CE coverage [29,43]. Table S1 summarizes the results from the aforementioned pieced of literature and this study. This observation suggests that the limited CE coverage primarily reflects intrinsic ionization and MS detection constraints rather

than an adverse effect of the aPB derivatization. Consistent with this interpretation, the number of annotated CE species in underivatized samples analyzed in positive ion mode was only marginally higher (13 species) than that obtained here after derivatization in negative ion mode (10 species) for human plasma. Together, these results demonstrate that aPB derivatization enables robust, quantitative, and regioisomer-resolved profiling of CE in complex biological matrices that is complementary to most MS-based lipidomics workflows as it employs negative-ion LC–MS/MS.

4. Conclusions

In this work, we demonstrated that aPB derivatization with 6-AU can be successfully extended to cholesteryl esters, enabling negative-ion-mode LC–MS/MS analysis with unambiguous localization of C=C bond regiochemistry. Despite the intrinsic challenges associated with the ionization and analysis of highly hydrophobic CE species, the optimized derivatization conditions afforded robust and reproducible generation of diagnostic fragment ions, including a previously unreported set of high-intensity fragments that proved particularly suitable for quantitative applications. To the best of our knowledge, this is the first report of the use of negative ionization HRMS for the annotation and quantitation of CE. The workflow enabled both relative and absolute quantitation of CE regioisomers with good linearity, repeatability, and trueness over a wide dynamic range. Importantly, the use of a single dominant diagnostic ion (F3) simplified data processing without compromising quantitative performance. Application to complex biological matrices demonstrated the feasibility of the approach in real samples, providing direct access to CE regioisomer distributions. The observed tissue-dependent differences in CE 18:1 isomer composition were consistent with known fatty acid metabolism, supporting the biochemical relevance of the obtained data.

Taken together, this study establishes aPB-based derivatization as a viable and complementary strategy for CE analysis. The workflow expands the analytical toolbox available for lipidomics studies where detailed molecular structure, rather than solely lipid class abundance, is critical for biological interpretation.

CRediT authorship contribution statement

Andrea Cerrato: Writing – original draft, Methodology, Formal analysis. **Enrico Taglioni:** Visualization, Investigation. **Chiara Cavaliere:** Writing – review & editing. **Aldo Laganà:** Supervision, Project administration. **Elena Lucà:** Investigation. **Carmela Maria Montone:** Writing – review & editing, Visualization. **Anna Laura Capriotti:** Writing – review & editing, Supervision, Project administration, Methodology, Conceptualization.

Declaration of competing interest

The authors declare that they have no known competing financial interests or personal relationships that could have appeared to influence the work reported in this paper.

Appendix A. Supplementary data

Supplementary data to this article can be found online at https://doi.org/10.1016/j.aca.2026.345392.

Data availability

Data will be made available on request.

References

[1] N.B. Myant, The metabolism of cholesterol, Elsevier, Biol. Cholest. Relat. Steroid. (1981) 227–298, https://doi.org/10.1016/B978-0-433-22880-6.50012-6.

[2] J. Guo, S. Chen, Y. Zhang, J. Liu, L. Jiang, L. Hu, K. Yao, Y. Yu, X. Chen, Cholesterol metabolism: physiological regulation and diseases, MedComm 5 (2024), https://doi.org/10.1002/mco2.476.

[3] K. Buhman, Mammalian acyl-CoA:cholesterol acyltransferases, Biochim. Biophys. Acta Mol. Cell Biol. Lipids 1529 (2000) 142–154, https://doi.org/10.1016/S1388-1981(00)00144-X.

[4] C.C. Schwartz, J.M. VandenBroek, P.S. Cooper, Lipoprotein cholesteryl ester production, transfer, and output in vivo in humans, J. Lipid Res. 45 (2004) 1594–1607, https://doi.org/10.1194/jlr.M300511-JLR200.

[5] H. Wang, D.-Q. Peng, New insights into the mechanism of low high-density lipoprotein cholesterol in obesity, Lipids Health Dis. 10 (2011) 176, https://doi.org/10.1186/1476-511X-10-176.

[6] M.J. Gerl, W.L.C. Vaz, N. Domingues, C. Klose, M.A. Surma, J.L. Sampaio, M. S. Almeida, G. Rodrigues, P. Araújo-Gonçalves, J. Ferreira, C. Borbinha, J.P. Marto, M. Viana-Baptista, K. Simons, O.V. Vieira, Cholesterol is inefficiently converted to cholesteryl esters in the blood of cardiovascular disease patients, Sci. Rep. 8 (2018) 14764, https://doi.org/10.1038/s41598-018-33116-4.

[7] N.L. Raftopulos, T.C. Washaya, A. Niederprüm, A. Egert, M.F. Hakeem-Sanni, B. Varney, A. Aishah, M.L. Georgieva, E. Olsson, D.Z. dos Santos, Z.D. Nassar, B. J. Cochran, S.R. Nagarajan, M.S. Kakani, J.F. Hastings, D.R. Croucher, K.-A. Rye, L. M. Butler, T. Grewal, A.J. Hoy, Prostate cancer cell proliferation is influenced by LDL-cholesterol availability and cholesteryl ester turnover, Cancer Metabol. 10 (2022) 1, https://doi.org/10.1186/s40170-021-00278-1.

[8] M. Elleder, A. Chlumská, J. Hyánek, H. Poupětová, J. Ledvinová, S. Maas, P. Lohse, Subclinical course of cholesteryl ester storage disease in an adult with hypercholesterolemia, accelerated atherosclerosis, and liver cancer, J. Hepatol. 32 (2000) 528–534, https://doi.org/10.1016/S0168-8278(00)80407-9.

[9] M. Mihajlovic, T. Gojkovic, S. Vladimirov, M. Miljkovic, A. Stefanovic, J. Vekic, D. Zeljkovic, B. Trifunovic, J. Kotur-Stevuljevic, V. Spasojevic-Kalimanovska, A. Zeljkovic, Changes in lecithin: cholesterol acyltransferase, cholesteryl ester transfer protein and paraoxonase-1 activities in patients with colorectal cancer, Clin. Biochem. 63 (2019) 32–38, https://doi.org/10.1016/j.clinbiochem.2018.11.010.

[10] M. Xiao, J. Xu, W. Wang, B. Zhang, J. Liu, J. Li, H. Xu, Y. Zhao, X. Yu, S. Shi, Functional significance of cholesterol metabolism in cancer: from threat to treatment, Exp. Mol. Med. 55 (2023) 1982–1995, https://doi.org/10.1038/s12276-023-01079-w.

[11] D. Schwudke, K. Schuhmann, R. Herzog, S.R. Bornstein, A. Shevchenko, Shotgun lipidomics on high resolution mass spectrometers, Cold Spring Harbor Perspect. Biol. 3 (2011), https://doi.org/10.1101/cshperspect.a004614 a004614–a004614.

[12] E.-M. Harrieder, F. Kretschmer, S. Böcker, M. Witting, Current state-of-the-art of separation methods used in LC-MS based metabolomics and lipidomics, J. Chromatogr. B 1188 (2022) 123069, https://doi.org/10.1016/j.jchromb.2021.123069.

[13] M. Lin, Z. Wang, D. Wang, X. Chen, J.-L. Zhang, Mathematical model-assisted UHPLC-MS/MS method for global profiling and quantification of cholesteryl esters in hyperlipidemic golden hamsters, Anal. Chem. 91 (2019) 4504–4512, https://doi.org/10.1021/acs.analchem.8b05337.

[14] J.A. Bowden, F. Shao, C.J. Albert, J.W. Lally, R.J. Brown, J.D. Procknow, A. H. Stephenson, D.A. Ford, Electrospray ionization tandem mass spectrometry of sodiated adducts of cholesteryl esters, Lipids 46 (2011) 1169–1179, https://doi.org/10.1007/s11745-011-3609-2.

[15] J.A. Bowden, C.J. Albert, O.S. Barnaby, D.A. Ford, Analysis of cholesteryl esters and diacylglycerols using lithiated adducts and electrospray ionization-tandem mass spectrometry, Anal. Biochem. 417 (2011) 202–210, https://doi.org/10.1016/j.ab.2011.06.015.

[16] P.M. Hutchins, R.M. Barkley, R.C. Murphy, Separation of cellular nonpolar neutral lipids by normal-phase chromatography and analysis by electrospray ionization mass spectrometry, J. Lipid Res. 49 (2008) 804–813, https://doi.org/10.1194/jlr.M700521-JLR200.

[17] R.S.E. Young, A.P. Bowman, K.D. Tousignant, B.L.J. Poad, J.H. Gunter, L.K. Philp, C.C. Nelson, S.R. Ellis, R.M.A. Heeren, M.C. Sadowski, S.J. Blanksby, Isomeric lipid signatures reveal compartmentalized fatty acid metabolism in cancer, J. Lipid Res. 63 (2022) 100223, https://doi.org/10.1016/j.jlr.2022.100223.

[18] A. Cerrato, C. Cavaliere, A. Laganà, C.M. Montone, S. Piovesana, A. Sciarra, E. Taglioni, A.L. Capriotti, First proof of concept of a click inverse electron demand diels–alder reaction for assigning the regiochemistry of carbon–carbon double bonds in untargeted lipidomics, Anal. Chem. 96 (2024) 10817–10826, https://doi.org/10.1021/acs.analchem.4c02146.

[19] J.R. Bonney, B.M. Prentice, Perspective on emerging mass spectrometry technologies for comprehensive lipid structural elucidation, Anal. Chem. 93 (2021) 6311–6322, https://doi.org/10.1021/acs.analchem.1c00061.

[20] P.E. Williams, D.R. Klein, S.M. Greer, J.S. Brodbelt, Pinpointing double bond and sn -Positions in glycerophospholipids via hybrid 193 nm ultraviolet photodissociation (UVPD) mass spectrometry, J. Am. Chem. Soc. 139 (2017) 15681–15690, https://doi.org/10.1021/jacs.7b06416.

[21] J.L. Campbell, T. Baba, Near-complete structural characterization of phosphatidylcholines using electron impact excitation of ions from organics, Anal. Chem. 87 (2015) 5837–5845, https://doi.org/10.1021/acs.analchem.5b01460.

[22] M.C. Thomas, T.W. Mitchell, D.G. Harman, J.M. Deeley, J.R. Nealon, S.J. Blanksby, Ozone-induced dissociation: elucidation of double bond position within mass-

selected lipid ions, Anal. Chem. 80 (2008) 303–311, https://doi.org/10.1021/ac7017684.
[23] J.P. Menzel, R.S.E. Young, A.H. Benfield, J.S. Scott, P. Wongsomboon, L. Cudlman, J. Cvačka, L.M. Butler, S.T. Henriques, B.L.J. Poad, S.J. Blanksby, Ozone-enabled fatty acid discovery reveals unexpected diversity in the human lipidome, Nat. Commun. 14 (2023) 3940, https://doi.org/10.1038/s41467-023-39617-9.
[24] X. Ma, L. Chong, R. Tian, R. Shi, T.Y. Hu, Z. Ouyang, Y. Xia, Identification and quantitation of lipid C=C location isomers: a shotgun lipidomics approach enabled by photochemical reaction, Proc. Natl. Acad. Sci. 113 (2016) 2573–2578, https://doi.org/10.1073/pnas.1523356113.
[25] D. Unsihuay, P. Su, H. Hu, J. Qiu, S. Kuang, Y. Li, X. Sun, S.K. Dey, J. Laskin, Imaging and analysis of isomeric unsaturated lipids through online photochemical derivatization of carbon–carbon double bonds, Angew. Chem. Int. Ed. 60 (2021) 7559–7563, https://doi.org/10.1002/anie.202016734.
[26] G. Feng, M. Gao, R. Fu, Q. Wan, T. Wang, Z. Zhang, S. Chen, Direct N-Me Aziridination Reaction Enables Pinpointing C=C Bonds in Lipids with Mass Spectrometry, 2022, https://doi.org/10.1101/2022.04.24.489320.
[27] G. Feng, M. Gao, H. Chen, Z. Zhang, J. Chen, Y. Tong, P. Wu, R. Fu, Y. Lin, S. Chen, Stable-isotope N-Me aziridination enables accurate quantitative C═C isomeric lipidomics, Anal. Chem. 96 (2024) 2524–2533, https://doi.org/10.1021/acs.analchem.3c04824.
[28] J. Ren, E.T. Franklin, Y. Xia, Uncovering structural diversity of unsaturated fatty acyls in cholesteryl esters via photochemical reaction and tandem mass spectrometry, J. Am. Soc. Mass Spectrom. 28 (2017) 1432–1441, https://doi.org/10.1007/s13361-017-1639-6.
[29] X. Xie, J. Zhao, M. Lin, J.-L. Zhang, Y. Xia, Profiling of cholesteryl esters by coupling charge-tagging paternò–büchi reaction and liquid chromatography–mass spectrometry, Anal. Chem. 92 (2020) 8487–8496, https://doi.org/10.1021/acs.analchem.0c01241.
[30] J. Sun, J. Luo, M. Gao, F. Wang, W. Nie, M. Chen, S. Chen, Quantum chemistry calculation-assisted large-scale collision cross section prediction empowers derivatization-enhanced multidimensional metabolomics, Angew. Chem. Int. Ed. 64 (2025), https://doi.org/10.1002/anie.202507483.
[31] A. Cerrato, A.L. Capriotti, C. Cavaliere, C.M. Montone, S. Piovesana, A. Laganà, Novel aza-paternò-büchi reaction allows pinpointing carbon–carbon double bonds in unsaturated lipids by higher collisional dissociation, Anal. Chem. 94 (2022) 13117–13125, https://doi.org/10.1021/acs.analchem.2c02549.
[32] A. Cerrato, S.E. Aita, G. Cannazza, C. Cavaliere, A. Cavazzini, C. Citti, C. M. Montone, E. Taglioni, A. Laganà, One-phase extraction coupled with photochemical reaction allows the in-depth lipid characterization of hempseeds by untargeted lipidomics, Talanta 271 (2024) 125686, https://doi.org/10.1016/j.talanta.2024.125686.
[33] C.M. Montone, C. Cavaliere, A. Cerrato, A. Laganà, S. Piovesana, E. Taglioni, A. L. Capriotti, Detailed lipid investigation of edible seaweeds by photochemical derivatization and untargeted lipidomics, Anal. Bioanal. Chem. 416 (2024) 6269–6282, https://doi.org/10.1007/s00216-024-05573-6.
[34] E.G. Bligh, W.J. Dyer, A rapid method of total lipid extraction and purification, Can. J. Biochem. Physiol. 37 (1959) 911–917, https://doi.org/10.1139/o59-099.
[35] S. Piovesana, C. Cavaliere, A. Cerrato, C.M.C.M. Montone, A. Laganà, A.L.A. L. Capriotti, Developments and pitfalls in the characterization of phenolic compounds in food: from targeted analysis to metabolomics-based approaches, TrAC Trends Anal. Chem. 133 (2020) 116083, https://doi.org/10.1016/j.trac.2020.116083.
[36] V. Declerck, D.J. Aitken, N -Aminoazetidinecarboxylic acid: direct access to a small-ring hydrazino acid, J. Org. Chem. 76 (2011) 708–711, https://doi.org/10.1021/jo102108t.
[37] J. Zhao, X. Xie, Q. Lin, X. Ma, P. Su, Y. Xia, Next-generation paternò–büchi reagents for lipid analysis by mass spectrometry, Anal. Chem. 92 (2020) 13470–13477, https://doi.org/10.1021/acs.analchem.0c02896.
[38] A.B. Falowo, V. Muchenje, A. Hugo, Effect of sous-vide technique on fatty acid and mineral compositions of beef and liver from Bonsmara and non-descript cattle, Ann. Anim. Sci. 17 (2017) 565–580, https://doi.org/10.1515/aoas-2016-0078.
[39] Y. Li, M. Amrutkar, A.V. Finstadsveen, K.T. Dalen, C.S. Verbeke, I.P. Gladhaug, Fatty acids abrogate the growth-suppressive effects induced by inhibition of cholesterol flux in pancreatic cancer cells, Cancer Cell Int. 23 (2023) 276, https://doi.org/10.1186/s12935-023-03138-8.
[40] D. Gowda, S.G.B. Gowda, A. Ikeda, R.M. Ketema, Y. Ait Bamai, R. Kishi, H. Chiba, S.-P. Hui, Quantitative determination of plasma cholesteryl ester levels in Japanese preadolescents from the Hokkaido study using liquid chromatography/tandem mass spectrometry, Steroids 211 (2024) 109498, https://doi.org/10.1016/j.steroids.2024.109498.
[41] M.J. Gerl, C. Klose, M.A. Surma, C. Fernandez, O. Melander, S. Männistö, K. Borodulin, A.S. Havulinna, V. Salomaa, E. Ikonen, C.V. Cannistraci, K. Simons, Machine learning of human plasma lipidomes for obesity estimation in a large population cohort, PLoS Biol. 17 (2019) e3000443, https://doi.org/10.1371/journal.pbio.3000443.
[42] Z. Vaňková, O. Peterka, M. Chocholoušková, D. Wolrab, R. Jirásko, M. Holčapek, Retention dependences support highly confident identification of lipid species in human plasma by reversed-phase UHPLC/MS, Anal. Bioanal. Chem. 414 (2022) 319–331, https://doi.org/10.1007/s00216-021-03492-4.
[43] J. Wang, X. Liu, P. Cao, S. Li, B. Hu, S. Jia, P. Yan, Z. Du, H. Jiang, Qualitative distribution of endogenous cholesteryl esters in plasma of humans and three rodent species using stepwise UPLC-Q-Exactive-MS, Curr. Med. Sci. 42 (2022) 692–701, https://doi.org/10.1007/s11596-022-2577-5.